THE JOURNAL OF BIOLOGICAL CHEMISTRY VOL. 284, NO. 8, pp. 5000–5009, February 20, 2009

Activation of Leukemia-associated RhoGEF by $G\alpha_{13}$ with Significant Conformational Rearrangements in the Interface*[S]

Received for publication, May 28, 2008, and in revised form, December 11, 2008 Published, JBC Papers in Press, December 12, 2008, DOI 10.1074/jbc.M804073200

Nobuchika Suzuki[‡§], Kouhei Tsumoto[¶], Nicole Hajicek[‖1], Kenji Daigo[‡], Reiko Tokita[§], Shiro Minami[§], Tatsuhiko Kodama[‡], Takao Hamakubo[‡], and Tohru Kozasa[‡‖2]

From the [‡]Laboratory of Systems Biology and Medicine, Research Center for Advanced Science and Technology, The University of Tokyo, Tokyo 153-8904, Japan, the [§]Department of Bioregulation, Nippon Medical School, and the [¶]Department of Medical Genome Sciences, Graduate School of Frontier Sciences, The University of Tokyo, Tokyo 277-8562, Japan, and the [‖]Department of Pharmacology, University of Illinois, Chicago, Illinois 60612

The transient protein-protein interactions induced by guanine nucleotide-dependent conformational changes of G proteins play central roles in G protein-coupled receptor-mediated signaling systems. Leukemia-associated RhoGEF (LARG), a guanine nucleotide exchange factor for Rho, contains an RGS homology (RH) domain and Dbl homology/pleckstrin homology (DH/PH) domains and acts both as a GTPase-activating protein (GAP) and an effector for $G\alpha_{13}$. However, the molecular mechanism of LARG activation upon $G\alpha_{13}$ binding is not yet well understood. In this study, we analyzed the $G\alpha_{13}$-LARG interaction using cellular and biochemical methods, including a surface plasmon resonance (SPR) analysis. The results obtained using various LARG fragments demonstrated that active $G\alpha_{13}$ interacts with LARG through the RH domain, DH/PH domains, and C-terminal region. However, an alanine substitution at the RH domain contact position in $G\alpha_{13}$ resulted in a large decrease in affinity. Thermodynamic analysis revealed that binding of $G\alpha_{13}$ proceeds with a large negative heat capacity change (ΔCp°), accompanied by a positive entropy change (ΔS°). These results likely indicate that the binding of $G\alpha_{13}$ with the RH domain triggers conformational rearrangements between $G\alpha_{13}$ and LARG burying an exposed hydrophobic surface to create a large complementary interface, which facilitates complex formation through both GAP and effector interfaces, and activates the RhoGEF. We propose that LARG activation is regulated by an induced-fit mechanism through the GAP interface of $G\alpha_{13}$.

Heterotrimeric G proteins[3] serve as key molecular switches to transduce a large array of extracellular signals into cells by actively alternating their conformations between GDP-bound inactive and GTP-bound active forms. In the current model, the ligand-activated G protein-coupled receptors (GPCRs) catalyze the exchange of GDP for GTP on $G\alpha$ subunits (1). Upon activation, three switch regions in the $G\alpha$ subunit undergo significant conformational changes, followed by dissociation of the GTP-bound $G\alpha$ subunit from the $G\beta\gamma$ subunits. Both $G\alpha$-GTP and free $G\beta\gamma$ interact with diverse downstream effectors to transmit intracellular signals. The $G\alpha$ subunit hydrolyzes bound GTP to GDP by its intrinsic GTPase activity. This deactivation process is further accelerated by GTPase-activating proteins (GAPs) such as regulator of G protein signaling (RGS) proteins (2, 3). $G\alpha$-GDP dissociates from effectors and re-associates with $G\beta\gamma$ to terminate the signal.

Although this model explains the basic concept of G protein signaling, the molecular dynamics of interactions among GPCR, G protein, RGS protein, and effector during the signaling process is not well understood. It has been suggested that the GPCR signals are integrated into the intracellular signaling network at the level of G proteins (4). Accumulating evidence suggests that the $G\alpha$ subunit acts as the core of the signaling complex at the membrane, which is formed through the transient protein-protein interactions of multiple signaling components (5, 6). Thus, the quantitative analysis of the dynamic molecular interactions in the GPCR signaling complex will be crucial to understanding various cellular processes.

* This work was supported, in whole or in part, by National Institutes of Health Grant GM61454 (to T. K.). This work was also supported by the American Heart Association (to T. K.), by Translational Systems Biology and Medicine Initiative from the Ministry of Education, Culture, Sports, Science and Technology of Japan, by the Program of Fundamental Studies in Health Science of the National Institute of Biomedical Innovation in Japan, and by the NFAT project of the New Energy and Industrial Technology Development Organization in Japan. The costs of publication of this article were defrayed in part by the payment of page charges. This article must therefore be hereby marked "*advertisement*" in accordance with 18 U.S.C. Section 1734 solely to indicate this fact.

[S] The on-line version of this article (available at http://www.jbc.org) contains supplemental text, Figs. S1–S5, and references.

[1] Supported by a Pharmacological Sciences Training Grant from the NIH and a pre-doctoral fellowship from the Greater Midwest Affiliate of the American Heart Association.

[2] To whom correspondence should be addressed: 835 S. Wolcott Ave., Chicago IL 60612. Tel.: 312-413-0111; Fax: 312-996-1225; E-mail: tkozas@uic.edu.

[3] The abbreviations used are: G protein, guanosine nucleotide-binding regulatory protein; GPCR, G protein-coupled receptor; GEF, guanine nucleotide exchange factor; LARG, leukemia-associated RhoGEF; RGS, regulator of G protein signaling; RH, RGS homology; DH, Dbl homology; PH, pleckstrin homology; GAP, GTPase-activating protein; SPR, surface plasmon resonance; SRE, serum response element; GTPγS, guanosine 5′-3-*O*-(thio)triphosphate; PLC, phospholipase C; PDEγ, the γ subunit of cGMP phosphodiesterase; aa, amino acid(s); WT, wild type; GST, glutathione *S*-transferase; Ni-NTA, nickel-nitrilotriacetic acid; RBD, Rhotekin Rho-binding domain.

$G\alpha_{12}$ and $G\alpha_{13}$ subunits have been demonstrated to regulate the activity of Rho GTPase through RhoGEFs, which contain an N-terminal RGS homology domain (RH-RhoGEFs) (7–10). RH-RhoGEFs, which consist of p115RhoGEF/Lsc, PDZ-RhoGEF/GTRAP48, and LARG in mammalian species, directly link the activation of GPCRs by extracellular ligands to the regulation of Rho activity in cells (10–14). All three RH-RhoGEFs contain an N-terminal RH domain, which specifically recognizes the active form of $G\alpha_{12}$ or $G\alpha_{13}$ and central DH/PH domains characteristic of GEFs for Rho GTPases. It has been demonstrated *in vitro* that LARG and p115RhoGEF serve as specific GAPs for $G\alpha_{12/13}$ through their RH domains and also as their effectors to regulate Rho GTPase activation (11–13). A structural study has demonstrated that the interface of the RH domain of p115RhoGEFs and a $G\alpha_{13/i1}$ chimera is different from that of the RGS domain of RGS4 and $G\alpha_{i1}$ (7). The N-terminal small element in the RH domain, which is required for GAP activity toward $G\alpha_{13}$, contacts the switch regions and the helical domain of the $G\alpha_{13/i1}$ chimera. The core module of the p115RhoGEF RH domain binds to the region of $G\alpha_{13/i1}$, which is conventionally used for effector binding. These results suggest roles for the RH domain in the stimulation of GEF activity by $G\alpha_{13}$ in addition to GAP activity. On the other hand, several studies have also indicated that regions outside of RH domain of RH-RhoGEFs, particularly the DH/PH domains, interact directly with activated $G\alpha_{13}$ (11, 14, 15). In addition, we have demonstrated recently that p115RhoGEF interacts with distinct surfaces of $G\alpha_{13}$ for the GAP reaction or GEF activity regulation (16). However, the molecular mechanism of LARG activation upon $G\alpha_{13}$ binding is not clearly understood.

In this study, we have developed a quantitative method for the kinetic and thermodynamic analysis of $G\alpha_{13}$-effector interaction using surface plasmon resonance (SPR) with sensor chips on which $G\alpha_{13}$ was immobilized. We examined the kinetics and thermodynamics of the $G\alpha_{13}$-LARG interaction and assessed LARG activation using both *in vitro* and cell-based approaches. We present evidence that, in addition to the interaction with the RH domain, the DH/PH domains and C-terminal region of LARG also interact with $G\alpha_{13}$ to form the high affinity $G\alpha_{13}$-LARG complex and activate RhoGEF activity. We further propose that LARG adopts the active conformation using an induced-fit mechanism through association with the GAP interface of $G\alpha_{13}$. A similar mechanism may also be used with other Gα-effector interactions.

EXPERIMENTAL PROCEDURES

Construction of Plasmids—Human LARG cDNA (NM 015313), mouse $G\alpha_{13}$ cDNA (NM 010303), and human p115RhoGEF (NM004706) were used in this study. Full-length LARG (FL-LARG) (aa 1–1544), LARG-RDPC (aa 307–1544), LARG-DPC (aa 617–1544), LARG-RDP (aa 307–1146), LARG-PDZ (aa 1–188), LARG-RH (aa 318–625), LARG-DH/PH (aa 607–1146), LARG-C (aa 1305–1544), PDZ-RhoGEF, FL-p115 (aa 1–912), and p115-RH (aa 1–252) were subcloned into the pcDNA-*myc* vector with an N-terminal *myc* tag (Fig. 1*A*). cDNAs encoding the wild-type $G\alpha_{13}$WT and the constitutively active $G\alpha_{13}$Q226L ($G\alpha_{13}$QL) mutant were subcloned into the pCMV5 vector. The $G\alpha_{13}$K204A ($G\alpha_{13}$KA) and $G\alpha_{13}$K204A/Q226L ($G\alpha_{13}$KA/QL) point mutants were generated in $G\alpha_{13}$WT or $G\alpha_{13}$Q226L, respectively, using the QuikChange site-directed mutagenesis kit as described previously (Stratagene) (15). cDNA encoding the human V14RhoA mutant was subcloned into the pCMV5-FLAG vector and used for cell-based assays.

Expression and Purification of Proteins—FL-LARG, LARG-RDPC, LARG-DPC, LARG-RDP, LARG-DH/PH, LARG-RH, LARG-C, and LARG-PDZ constructs were subcloned into the pFastBacHT transfer vector with a six-histidine tag at the N terminus (Invitrogen), and their recombinant baculoviruses were generated. Recombinant $G\alpha_{13}$ wild-type ($G\alpha_{13}$WT), His_6-geranylgeranylated RhoA (gg-RhoA), and His_6-LARG proteins were purified using the Sf9-baculovirus expression system as described before (17). His_6-$G\alpha_{i/13}$ or -$G\alpha_{i/13}$K204A chimeric protein, with the N-terminal coding region of rat $G\alpha_{i1}$ (residues 1–28), and the backbone of $G\alpha_{13}$WT or $G\alpha_{13}$K204A (residues 47–377) were purified from Sf9 cells as described (9). This substitution of the N-terminal helix of $G\alpha_{i1}$ for the corresponding region of $G\alpha_{13}$ has been shown to facilitate the production of functional protein retaining the specific biochemical properties of wild-type $G\alpha_{13}$. For SPR assays, the His_6 tags of LARG, $G\alpha_{i/13}$, and $G\alpha_{i/13}$KA were removed by digestion with tobacco etch virus protease for 8 h at 4 °C.

SPR Assays—SPR measurements were carried out using a Biacore 3000 and a Biacore T100. $G\alpha_{i/13}$ and $G\alpha_{i/13}$KA proteins were immobilized on parallel channels of the Biacore sensor chip CM5 using amine coupling chemistry according to the manufacturer's protocol. The coupling reactions were performed at 5 μl/min at 25 °C using Running Buffer AMF (−) (10 mM Hepes, pH 7.4, 150 mM NaCl, 3 mM EDTA, 0.005% Surfactant P20, 4 mM $MgCl_2$, 10 μM GDP, 1 mM dithiothreitol, 30 [micro]M $AlCl_3$, 10 mM $MgCl_2$, 10 mM NaF). All flow cell surfaces were activated by a 1:1 mixture of *N*-hydroxy-succinimide/1-ethyl-3-(3-dimethylaminopropyl) carbodiimide for 7 min, followed by injection of $G\alpha_{i/13}$ or $G\alpha_{i/13}$KA diluted to 10 μg/ml in Ligand Dilution Buffer (10 mM sodium acetate, pH 6.0, 1 mM $MgCl_2$, 10 μM GDP, 1 mM dithiothreitol) to a density of ~4000 relative units. Residual binding sites on the surface were blocked with a 7-min injection of 1 M ethanolamine.

Kinetic binding analysis was performed at 15 °C. Immobilized $G\alpha_{i/13}$ or $G\alpha_{i/13}$KA on a biosensor chip, which was in an inactive form in the absence of AMF (30 μM $AlCl_3$/10 mM $MgCl_2$/10 mM NaF), was activated by AMF in running buffer. Samples of serially diluted LARG proteins at five to six steps were injected over the inactivated or activated $G\alpha_{i/13}$ and $G\alpha_{i/13}$KA surfaces using Running Buffer AMF (−) or Running Buffer AMF (+) (10 mM Hepes, pH 7.4, 150 mM NaCl, 3 mM EDTA, 0.005% surfactant P20, 10 mM $MgCl_2$, 10 μM GDP, 1 mM dithiothreitol, 10 mM NaF, 30 μM $AlCl_3$) and reference flow cells at a flow rate of 10 μl/min for 1 min followed by 2-min dissociation using KINJECT mode. The sensor surfaces were regenerated by the injection of Regeneration Buffer (1 N NaCl, 1 mM $MgCl_2$, 10 μM GDP, 1 mM dithiothreitol) after each binding cycle. All data were corrected for nonspecific binding and buffer shifts by double subtracting binding responses collected from a blank reference cell and a buffer injection over a $G\alpha_{i/13}$ or $G\alpha_{i/13}$KA immobilized flow cell. Data were fitted to a simul-

taneous k_a/k_d, 1:1 binding, and Global fitting using the BIAevaluation program. Kinetic analyses were not performed when the responses were <1/10 compared with those with $G\alpha_{i/13}$ in the presence of AMF. The experiments were performed more than four times. Thermodynamic experiments were done at a range of temperatures from 7 °C to 15 °C in 2° increments. Six different concentrations of LARG proteins were used for each temperature.

Thermodynamic Data Analysis—At an equilibrium state, the thermodynamic parameters, $\Delta H°$ (enthalpy change), $\Delta S°$ (entropy change), $\Delta G°$ (free energy change), and $\Delta Cp°$ (heat capacity change) were derived from the van't Hoff equation, which states that $\Delta G° = \Delta H° - T\Delta S° = RT\ln K_D$, by measuring the temperature dependence of K_D (equilibrium constant). Such parameters determined by the van't Hoff method are demonstrated to agree with those determined directly using calorimetry (18–20). If ΔH and ΔS have significant temperature dependence and ΔCp was assumed to be independent of temperature over a short temperature range, the relationship between the parameters becomes,

$$RT\ln K_D = \Delta H°_{T0} - T\Delta S°_{T0} + \Delta C_p°(T - T_0) - T\Delta C_p°\ln(T/T_0) \quad \text{(Eq. 1)}$$

with T_0 defined as the reference temperature (25 °C). The thermodynamic parameters in this study were calculated by fitting the data to Equation 1 using BiacoreT100 software.

For thermodynamic analysis of a transition state, the Eyring theory was employed (21),

$$\ln(k/T) = -\Delta G°^{\ddagger}/RT + \ln(k_B/\hbar) = \Delta S°^{\ddagger}/R - \Delta H°^{\ddagger}/RT + \ln(k_B/\hbar) \quad \text{(Eq. 2)}$$

where the ‡ symbol denotes the transition state, k is the association or dissociation constant, k_B is the Boltzmann constant, and $\hbar$ is the Planck constant. According to Equation 2, the thermodynamic parameters at association and dissociation were calculated by linear fitting by measuring k_a and k_d at several temperatures using BiacoreT100 software.

Binding of LARG Proteins with His-$G\alpha_{i/13}$ Immobilized on Ni-NTA-Agarose—COS1 cells were transfected using the Lipofectamine PLUS reagent with the indicated LARG constructs: *myc*-LARG-DPC (8 μg) and *myc*-RH (4 μg). Transfected cells were incubated at 37 °C in 10% CO_2 for 24 h. Cells were lysed with 650 ml of 1.25 × lysis buffer B (50 mM Tris-HCl, pH 7.5/150 mM NaCl/1% Nonidet P-40/0.5 mM EDTA/9.8 mM 2-mercaptoethanol/10 mM β-glycerophosphate/10 mM Na_3VO_4/10 mM $MgCl_2$/100 μM ATP/30 μM GDP/protease inhibitors) and centrifuged at 100,000 × *g* for 30 min. Equal amounts of supernatants were separated and incubated with 1.4 μg of His-$G\alpha_{i/13}$ immobilized on 5 μl of Ni-NTA-agarose beads in 1 × lysis buffer B with or without AMF for 60 min at 4 °C. The mixtures were washed three times 1 × lysis buffer B with or without AMF. The relative amount of LARG fragments bound to the activated- or deactivated-$G\alpha_{i/13}$ was visualized by immunoblot analysis using anti-Myc antibody.

Statistical Analysis—Data represent the mean ± S.E. of at least three independent experiments. Statistical significance of the difference was assigned based on results of Student's *t* test (Figs. 2*C* and 3*D*), or analysis of variance followed by Fisher's protected least significant difference test (Fig. 3*b*) (*, $p < 0.05$). Actual *n* and *p* values are provided in each figure legend.

Other Procedures—Co-immunoprecipitations, SRE-luciferase assays, subcellular localization of LARG, measurement of Rho activation in cells, cell rounding assays, and *in vitro* RhoGEF assays were performed as described before (9, 13). Details of these procedures are described in the supplemental information.

RESULTS

Direct Interaction of LARG with $G\alpha_{13}$ through Its RH Domain, DH/PH Domains, and C-terminal Region—We first examined the ability of several deletion constructs of LARG to interact with $G\alpha_{13}$ by co-immunoprecipitation using COS1 cells that were transiently transfected with *myc*-tagged LARG mutants and $G\alpha_{13}$ (Fig. 1, *A* and *B*). As previously reported, LARG-RDPC and LARG-RH, which contain the RH domain, preferentially bound to AMF-activated $G\alpha_{13}$, whose conformation resembles that of the transition state for GTP hydrolysis (15, 22). Intriguingly, $G\alpha_{13}$ also co-immunoprecipitated with LARG constructs without the RH domain: LARG-DPC, LARG-DH/PH, and LARG-C. Although the amount of co-immunoprecipitated $G\alpha_{13}$ was much lower than with LARG-RDPC or LARG-RH, the interaction with these LARG fragments was still dependent on activation of $G\alpha_{13}$. We reproducibly observed a small but significant increase in the amount of precipitated $G\alpha_{13}$ with LARG-C in response to $G\alpha_{13}$ activation. These results suggested that LARG might also interact with activated $G\alpha_{13}$ through the DH/PH domains and/or C-terminal region.

We thus examined the direct interaction between LARG and $G\alpha_{13}$ using an SPR method. We have recently constructed a $G\alpha_{i/13}$ chimera by substituting the N-terminal α1 helix of $G\alpha_{i1}$ for the corresponding region of $G\alpha_{13}$ and demonstrated that this $G\alpha_{i/13}$ protein purified by an Sf9-baculovirus expression system retains the same biochemical properties as wild-type $G\alpha_{13}$ for binding and hydrolysis of guanine nucleotides, activation of RH-RhoGEFs, and GAP response (9) (supplemental Fig. S1).

For the SPR analysis, $G\alpha_{i/13}$ was immobilized on the biosensor chip by amine coupling. The interaction of LARG fragments with $G\alpha_{i/13}$ on the sensor chip was analyzed by Biacore3000. An advantage of this method is that the affinity difference of an effector for the active or inactive $G\alpha_{13}$ can be quantitatively analyzed by the addition or exclusion of AMF in buffer on the same $G\alpha_{i/13}$ chip. For the kinetic analysis, the concentrations of LARG fragments as analytes were different for each construct. Thus, it should be noted that we cannot evaluate the binding affinity between different LARG proteins by comparing the amplitudes of the SPR responses.

Consistent with the cellular assays, the SRP assay clearly demonstrated that LARG-RH, LARG-DH/PH, and LARG-C preferentially interact with the active form of $G\alpha_{i/13}$ (Fig. 1*C* and Table 1). Because FL-LARG was sensitive to degradation during the assay, we exploited LARG-RDPC instead of FL-LARG for further analysis. LARG-RDPC showed kinetic parameters similar to FL-LARG in the presence of ALF_4^-. For

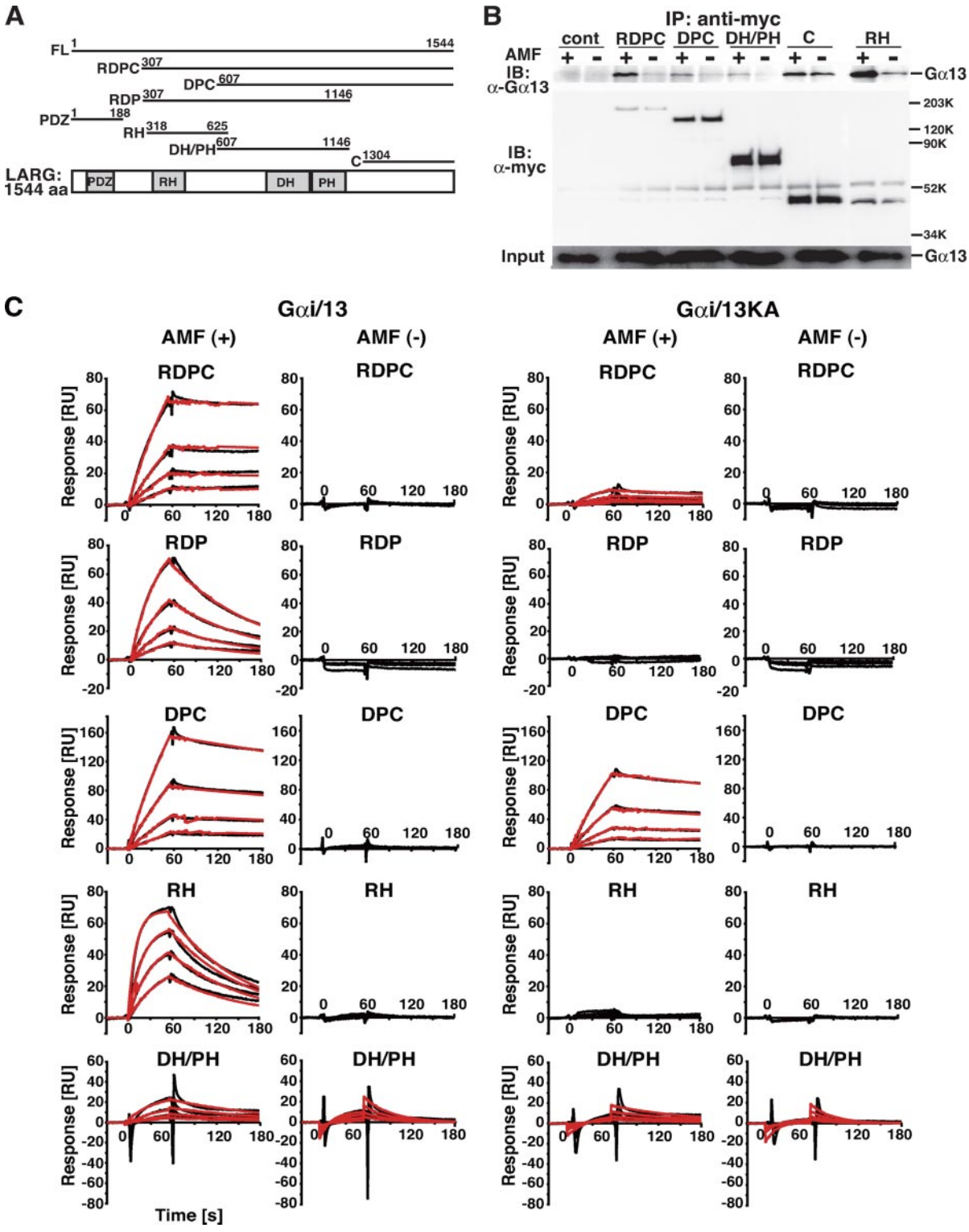

FIGURE 1. **Direct interaction of LARG with Gα$_{13}$ through its RH domain, DH/PH domains, and C-terminal region.** *A*, schematic representation of LARG and its deletion constructs. The amino acid numbers encoded in each constructs are listed. *PDZ*, PDZ domain; *RH*, RGS homology domain; *DH*, Dbl homology domain; *PH*, pleckstrin homology domain. A full-length, RDPC, DPC, RDP, PDZ, RH, DH/PH, or C-terminal region of LARG is referred to as *LARG-FL*, *-RDPC*, *-DPC*, *-RDP*, *-PDZ*, *-RH*, *-DH/PH*, or *-C*, respectively. *B*, the binding of various LARG proteins to Gα$_{13}$ in COS1 cells. COS1 cells were co-transfected with Gα$_{13}$WT (0.5 μg) and the indicated *myc*-tagged LARG constructs: RDPC (5 μg), DPC (4 μg), DH/PH (3 μg), C (4 μg), and RH (5 μg). The LARG proteins were immunoprecipitated by anti-Myc antibody from cell lysates in the presence or absence of AMF. Immunoprecipitates were separated by SDS-PAGE, followed by Western blotting using anti-Gα$_{13}$ antibody or anti-Myc antibody. *C*, kinetics of binding of LARG to Gα$_{i/13}$ or Gα$_{i/13}$KA immobilized on the SPR biosensor. Gα$_{i/13}$ and Gα$_{i/13}$KA proteins were immobilized on parallel channels of the Biacore sensor chip CM5 as described under "Experimental Procedures." The association phase of the reaction between serially diluted LARG fragments and Gα$_{i/13}$ was 2 min, and the dissociation phase was 1 min at 15 °C. The interactions were measured using Biacore 3000. *Black lines* show the experimental data. *Red lines* show fitting data analyzed as simultaneous k_a/k_d, 1:1 binding, and global fitting using the BIAevaluation program. In the absence of AMF, kinetic analyses were not performed when the responses were <1/10 of those with Gα$_{i/13}$ in the presence of AMF. The concentrations of proteins were: FL, 1.1–17.5 nM; RDPC, 4.4–70 nM; RDP, 1.1–17.5 nM; DPC, 37.5–600 nM; RH, 8.8–140 nM; and DH/PH, 78.1 nM to 1.25 μM.

TABLE 1

Kinetic parameters of LARG mutants binding to Gα$_{i/13}$ or Gα$_{i/13}$KA

k_a, association rate constant; k_d, dissociation rate constant; $K_D = k_d/k_a$, equilibrium constant. Kinetic properties were estimated from BIAcore raw data (four to five serial dilutions for each protein) using BIAevaluation software, as indicated in Fig. 1*C*.

Protein	ALF	$Ga_{i/13}$			$Ga_{i/13}$KA		
		k_a	k_d	K_D	k_a	k_d	K_D
		$M^{-1}s^{-1}$	s^{-1}	M	$M^{-1}s^{-1}$	s^{-1}	M
RDPC	−	ND[a]	ND	ND	ND	ND	ND
	+	4.4×10^5	3.0×10^{-4}	6.8×10^{-10}	2.9×10^5	6.5×10^{-3}	2.6×10^{-8}
RDP	−	ND	ND	ND	ND	ND	ND
	+	9.8×10^5	8.6×10^{-3}	8.8×10^{-9}	ND	ND	ND
DPC	−	ND	ND	ND	ND	ND	ND
	+	1.8×10^4	1.4×10^{-3}	7.6×10^{-8}	1.8×10^4	1.4×10^{-3}	8.1×10^{-8}
RH	−	ND	ND	ND	ND	ND	ND
	+	6.9×10^5	9.7×10^{-3}	1.5×10^{-8}	ND	ND	ND
DH/PH	−	2.7×10^4	2.8×10^{-2}	1.1×10^{-6}	3.7×10^4	3.2×10^{-2}	8.5×10^{-7}
	+	1.7×10^4	7.1×10^{-3}	4.3×10^{-7}	2.0×10^4	8.5×10^{-3}	4.3×10^{-7}
C	−	2.1×10^4	2.0×10^{-2}	9.6×10^{-7}	1.3×10^4	1.5×10^{-2}	1.1×10^{-6}
	+	2.4×10^4	8.6×10^{-3}	3.6×10^{-7}	9.4×10^3	9.9×10^{-3}	1.0×10^{-6}
PDZ	−	7.2×10^3	1.6×10^{-2}	2.2×10^{-6}	8.7×10^3	1.4×10^{-2}	1.6×10^{-6}
	+	5.0×10^3	1.3×10^{-2}	2.5×10^{-6}	3.9×10^3	1.1×10^{-2}	2.9×10^{-6}

[a] ND, the kinetic analysis was not done because the responses were less than 1/10 compared to those with Gα$_{i/13}$ in the presence of ALF^-.

LARG-FL *versus* LARG-RDPC: k_a (association rate constant) = 6.0×10^5 *versus* 4.4×10^5 M^{-1} s^{-1}, k_d (dissociation rate constant) = 8.1×10^{-4} *versus* 3.0×10^{-4} s^{-1}, and K_D (the equilibrium dissociation constant) = 1.4×10^{-9} *versus* 6.8×10^{-10} M.

The affinity of LARG-RDP or LARG-RDPC for activated Gα$_{i/13}$ was ~2-fold or 20-fold higher than the RH domain alone, respectively (Table 1). This suggests that the DH/PH domains and the C-terminal region of LARG may contribute to forming the high affinity Gα$_{i/13}$-LARG complex together with the RH domain. In particular, the C-terminal region of LARG greatly decreased the rate of dissociation of the Gα$_{i/13}$-LARG complex. In the presence of the C-terminal region, k_d was reduced by >5-fold (Table 1).

We have previously demonstrated that the mutation of lysine 204 to alanine in the switch I region of Gα$_{13}$ significantly reduces its affinity for LARG and its sensitivity to the GAP activity of LARG (8, 9, 15). To further characterize the role of the RH domain in the Gα$_{13}$-LARG interaction, we compared the binding kinetics of LARG fragments with Gα$_{i/13}$KA and Gα$_{i/13}$, which are immobilized on separate channels of the same biosensor chip (Fig. 1*C* and Table 1). Consistent with our previous result, the binding of LARG-RH to Gα$_{i/13}$ was abolished by the K204A mutation. In contrast, the interaction of LARG-DH/PH or LARG-DPC with Gα$_{i/13}$ was not affected by the K204A mutation (Table 1). These results indicate the existence of an interaction between Gα$_{13}$ and the DH/PH domains. It is also important to note that the KA mutation in Gα$_{13}$ significantly reduced the affinity for LARG fragments containing the RH domain but did not change the affinity for LARG-DH/PH and LARG-DPC. Thus, the initial association of the RH domain with Gα$_{13}$ might be necessary to induce the proper conformational change in LARG to form a high affinity complex with Gα$_{13}$.

Stimulation of the RhoGEF Activity of LARG through Direct Interaction between the DH/PH Domains and Gα$_{13}$—We next examined whether the interaction of Gα$_{13}$ with the DH/PH domains of LARG induces RhoGEF activation. First, we co-expressed LARG mutants lacking the RH domain with a constitutively active, GTPase-deficient mutant of Gα$_{13}$ (Gα$_{13}$Q226L) in HeLa cells and assayed SRF activation of the cell lysates as an indicator of Rho activation. The SRF activity of cell lysates expressing LARG-DH/PH or LARG-DPC was further stimulated in the presence of Gα$_{13}$QL similar to LARG-RDPC (Fig. 2*A*). The immunoblot of the transfected cell lysates showed similar expression levels of LARG constructs (Fig. 2*D*). However, the co-expression of Gα$_{13}$WT didn't synergistically potentiate the SRF activity stimulated by LARG-DPC or LARG-RDPC (supplemental Fig. S2). We also examined the amount of GTP-bound Rho in cells using GST-RBD pulldown assays (13, 23). Consistent with Fig. 2*A*, GTP-bound Rho in cells expressing LARG-DH/PH, LARG-DPC, or LARG-RDPC increased with the co-expression of Gα$_{13}$QL (Fig. 2*B*).

We then examined the stimulation of the GEF activity of the DH/PH domains by *in vitro* reconstitution assays using recombinant wild-type Gα$_{i/13}$ (Gα$_{13}$WT) and LARG proteins (13). AMF-activated Gα$_{i/13}$WT stimulated the RhoGEF activity of LARG-RDPC (Fig. 2*C*). However, in contrast to the results from cellular assays, Gα$_{i/13}$WT did not significantly stimulate the activity of LARG-DH/PH (Fig. 2, *B* and *C*). The lower binding affinity of LARG-DH/PH for Gα$_{i/13}$ compared with LARG-DPC (K_D: 4.3×10^{-7} M *versus* 7.6×10^{-8} M, respectively) may be responsible for this discrepancy.

The effect of co-expression of Gα$_{13}$QL on the subcellular distribution of LARG mutants was also examined under the same conditions as for the SRF assays in Fig. 2 (*A* and *D*). All of the LARG constructs were distributed mainly in cytosolic fractions in the absence of Gα$_{13}$QL. In the presence of Gα$_{13}$QL, LARG-RDPC, the only construct with a RH domain, was redistributed to the membrane fraction. LARG-RH was recruited to the membrane fraction in the presence of Gα$_{13}$QL, but not Gα$_{13}$WT or Gα$_{13}$KA (supplemental Fig. S3). These data suggest that the interaction of LARG-RH with activated Gα$_{13}$ is likely to be important for inducing membrane distribution of LARG similar to the case of p115RhoGEF (5). Thus, it is suggested that Gα$_{13}$ may regulate LARG activity through two distinct mechanisms, by inducing its membrane translocation through the RH domain and by stimulating its GEF activity through the DH/PH domains.

To confirm these results in a more physiological context, we performed cell rounding assays as an indicator of Rho activa-

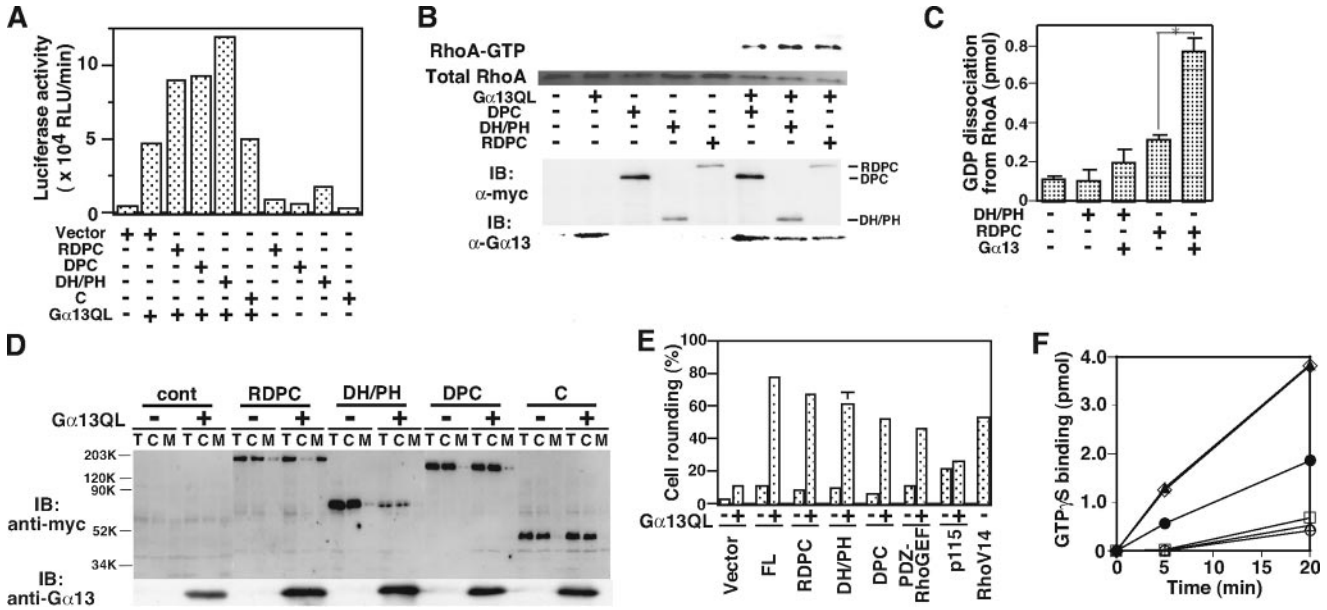

FIGURE 2. **RhoGEF activation of LARG by the direct interaction of the DH/PH domains with $G\alpha_{13}$.** *A*, potentiation of SRF activation by LARG with $G\alpha_{13}$. HeLa cells were cotransfected with 0.1 μg of SRE-luciferase reporter plasmid and the indicated constructs: $G\alpha_{13}$QL (0.01 μg), *myc*-LARG-RDPC (0.1 μg), *myc*-LARG-DPC (0.1 μg), *myc*-LARG-DH/PH (0.01 μg), and *myc*-LARG-C (0.1 μg). SRF activities of cell lysates were measured 24 h after transfection as described in the supplemental materials. *B*, RhoA activation by LARG-DH/PH with $G\alpha_{13}$ in HeLa cells. HeLa cells were transiently transfected with the indicated plasmids: $G\alpha_{13}$QL (1 μg), *myc*-tagged RDPC (10 μg), *myc*-DPC (1 μg), and *myc*-DH/PH (0.5 μg). The cells were serum-starved for 24 h after 5 h of transfection. Endogenous RhoA in the GTP-bound form was isolated using GST-Rhotekin RBD from the cell lysates as described in the supplemental materials. The expression of Myc-tagged LARG constructs and $G\alpha_{13}$ were analyzed by Western blotting using anti-Myc and anti-$G\alpha_{13}$ antibodies. *C*, *in vitro* RhoGEF assays of LARG-DH/PH and -RDPC. GDP dissociation from RhoA was measured at 20 °C after 2-min incubation in the presence of the indicated proteins: LARG-RDPC (20 nM), LARG-DH/PH (30 nM), AlF_4^--activated $G\alpha_{13}$WT (100 nM). (Student's *t* test: $n = 4$, *, $p < 0.001$). *D*, recruitment of LARG with RH domain to the plasma membrane by constitutively active $G\alpha_{13}$. HeLa cells were cotransfected in the same procedure as in Fig. 2*A*. The expression of LARG constructs in total cell lysate (*T*), crude cytosolic (*C*), and membrane (*M*) fractions, and $G\alpha_{13}$ in total lysates was detected by immunoblotting using anti-Myc antibody or anti-$G\alpha_{13}$ antibody. *E*, cell rounding induced by LARG constructs with the constitutively active $G\alpha_{13}$ in MDCKII cells. MDCKII cells were transiently transfected with the indicated *myc*-tagged LARG constructs in the presence or absence of $G\alpha_{13}$QL, or FLAG-tagged V14RhoA alone. The cells were serum-starved for 24 h after 5 h of transfection, then fixed, and triply stained with anti-Myc antibody, anti-$G\alpha_{13}$ antibody, and phalloidin for filamentous actin. Transfected cells were visualized by fluorescence microscopy, identified, and scored for rounding indicating the involvement of RhoA activation as described under the supplemental materials. The values were calculated from four independent experiments. The *images* are in supplemental Fig. S4. *F*, stimulation of the RhoGEF activity of LARG by $G\alpha_{i/13}$KA. GTPγS binding to RhoA (200 nM) was measured at 20 °C after 5-min incubation in the presence of the following proteins: ○, control; △, AlF_4^--activated $G\alpha_{i/13}$ (100 nM); □, AMF-activated $G\alpha_{i/13}$KA (100 nM); ●, RDPC (10 nM); ▲, RDPC (10 nM) plus AMF-activated $G\alpha_{i/13}$ (100 nM); ◇, RDPC (10 nM) plus AMF-activated $G\alpha_{i/13}$KA (100 nM).

tion (24). MDCKII cells were co-transfected with *myc*-tagged RH-RhoGEF constructs and $G\alpha_{13}$QL. In the presence of $G\alpha_{13}$QL, LARG-DH/PH or LARG-DPC induced cell rounding to a level similar to that observed with LARG-RDPC (Fig. 2*E* and supplemental Fig. S4). We further examined the role of lysine 204 in stimulating the GEF activity of LARG constructs. Unexpectedly, the GEF activity of LARG-RDPC was still stimulated by ALF_4^--activated $G\alpha_{i/13}$KA in the reconstitution assay (Fig. 2*F*). These results further support the existence of a direct interaction of $G\alpha_{13}$ with the DH/PH domains of LARG for RhoGEF activation.

Functional Roles of the RH Domain and C-terminal Region in RhoGEF Activation Mediated by the DH/PH Domains—We next examined the effect of the isolated RH domain or C-terminal region on the $G\alpha_{13}$-stimulated RhoGEF activity of DH/PH domains. GST-RBD pulldown assays demonstrated that co-expression of LARG-RH, but not p115RhoGEF-RH, potentiated the RhoGEF activity of LARG-DH/PH stimulated by $G\alpha_{13}$QL (Fig. 3*A*). In the reconstitution assay, the $G\alpha\iota/13$-stimulated RhoGEF activity of LARG-DH/PH was also significantly potentiated by the addition of LARG-RH to the reaction (Fig. 3*B*). However, RhoGEF activity of LARG-DH/PH was not stimulated by $G\alpha_{13}$ without the RH domain even at a higher concentration (120 nM). These results and the higher affinity of LARG-RDP *versus* LARG-RH or LARG-DH/PH for $G\alpha_{i/13}$ (Table 1) suggest that, even though the effect of these separated domains is less than that of the combined molecule, the RH-$G\alpha_{13}$ interaction increases the affinity of the DH/PH domains for $G\alpha_{13}$.

We then examined the binding of Myc-tagged LARG-RH and LARG-DPC expressed in COS1 cells to His-$G\alpha_{i/13}$ immobilized on Ni-NTA-agarose resin. The binding of LARG-DPC to AlF_4^--activated $G\alpha_{i/13}$ was dependent on the presence of LARG-RH (Fig. 3*C*). In addition, although the amount of bound LARG-DPC was much lower than that of LARG-RH, the presence of LARG-DPC and LARG-RH enhanced their binding to $G\alpha_{i/13}$. With $G\alpha_{i/13}$KA-resin, reduced binding of LARG-RH without LARG-DPC was observed, which is consistent with the results of the SPR analysis (Table 1). These results suggest that the RH domain and DH/PH domains simultaneously bind to $G\alpha_{13}$ through separate interfaces and that the binding of the RH domain with $G\alpha_{13}$ would enhance the affinity of the DH/PH domains for $G\alpha_{13}$.

We also investigated how the interaction of the C-terminal region of LARG with $G\alpha_{13}$ affects the RhoGEF activity using *in vitro* reconstitution assays (Fig. 3*D*). The addition of LARG-C fragment did not potentiate the GEF activity of LARG-RDP stimulated by $G\alpha_{i/13}$. Nevertheless, the RhoGEF activity of

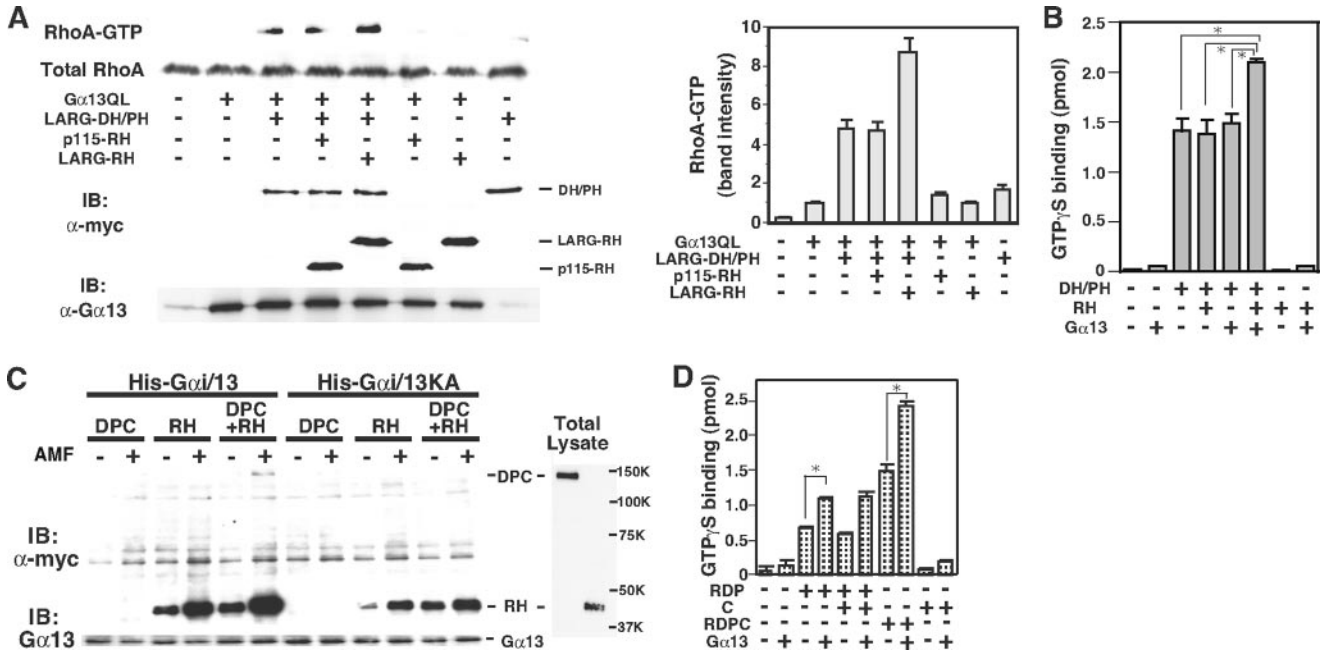

FIGURE 3. **Functional roles of the RH domain and C-terminal region for DH/PH domains-mediated GEF activation of LARG.** *A*, Enhancement of the $G\alpha_{13}$-stimulated RhoGEF activity of LARG-DH/PH by LARG-RH in HeLa cells. HeLa cells were transiently transfected with the indicated plasmids: $G\alpha_{13}$QL (1 μg), *myc*-tagged LARG-DH/PH (1.5 μg), *myc*-LARG-RH (2 μg), or *myc*-p115-RH (0.02 μg). GTP-bound form of RhoA was isolated as described in Fig. 2*B*. The *left* of the *panel* is a representative result from three independent experiments. The *right panel* shows the mean ± S.E. of values of amount of GTP-RhoA scanned using ImageJ program. *B*, potentiation of the $G\alpha_{13}$-induced RhoGEF activity of LARG-DH/PH by LARG-RH *in vitro*. GTPγS binding to RhoA (200 nM) was measured at 20 °C after 5-min incubation in the presence of the indicated proteins: AMF-activated $G\alpha_{13}$ (100 nM), RH (600 nM), DH/PH (120 nM). (Fisher's protected least significant difference test: $n = 3$, *, $p < 0.001$). *C*, enhancement of the binding of LARG-RH and LARG-DPC with $G\alpha_{13}$ immobilized on Ni-NTA-agarose. Equal amounts of cell lysates of COS1 cells transfected with *myc*-LARG-DPC (8 μg) or *myc*-LARG-RH (4 μg) were incubated with 1.4 μg of immobilized His-$G\alpha_{i/13}$ or His-$G\alpha_{i/13}$KA proteins onto Ni-NTA agarose beads in the presence or absence of AMF. The relative amount of LARG fragments bound to the activated- or deactivated-$G\alpha_{13}$ was visualized by Western blot analysis using anti-Myc antibody. The expression of the LARG proteins in total cell lysates and the $G\alpha_{13}$ protein in the reaction mixtures are also shown. *D*, the role of LARG C terminus in RhoGEF activation of LARG by $G\alpha_{13}$. GTPγS binding to RhoA (200 nM) was measured at 20 °C after 5-min incubation in the presence of the indicated proteins: AMF-activated $G\alpha_{13}$ (100 nM), RDP (20 nM), C (200 nM), and RDPC (20 nM) (Student's *t* test: $n = 3$, *, $p = 0.0001$).

LARG-RDPC was potentiated 2.5-fold compared with that of LARG-RDP, suggesting that the interaction of the C-terminal region with $G\alpha_{13}$ might also be involved in the conformational change of the LARG molecule to activate the RhoGEF activity.

In summary, these results strongly indicate that the multiple interactions of LARG with $G\alpha_{13}$ through its RH domain, DH/PH domains, and the C-terminal region coordinate together to form the active $G\alpha_{13}$-LARG signaling complex. The association of the RH domain with the $G\alpha_{13}$ surface, including Lys-204 likely induces the conformational change of the DH/PH domains of LARG necessary to stimulate RhoGEF activity.

Thermodynamic Analysis of the Interaction between $G\alpha_{13}$ and LARG—To further elucidate the dynamics of the conformational changes induced by $G\alpha_{13}$-LARG binding, especially the contribution of the RH domain or the DH/PH domains of LARG to the interaction with $G\alpha_{13}$, we determined the thermodynamic parameters of LARG-RH/$G\alpha_{13}$ and LARG-RDP/$G\alpha_{13}$ interactions by SPR analysis. The SPR analysis at several different temperatures from 7 °C to 15 °C was performed with a chip on which $G\alpha_{i/13}$ was immobilized using BiacoreT100 as described under "Experimental Procedures." Thermodynamic parameter (free energy $G°$, enthalpy $H°$, entropy $S°$, or heat capacity $Cp°$) changes at equilibrium state were calculated from the temperature dependence of K_D using the van't Hoff equation (Table 2). The thermodynamic parameters at equilibrium estimated from SPR analysis have been consistent with those determined directly using isothermal titration calorimetry (18–20). The parameters for the transition state of the interactions were calculated by the Eyring theory using the temperature dependence of association rate constant (k_a) or dissociation rate constant (k_d) as described under "Experimental Procedures" (21). The temperature dependence of K_D, k_a, and k_d from SPR analysis fit well with the theoretical equations (Fig. 4*A* and supplemental Fig. S5*A*).

TABLE 2

Thermodynamic characterization of the interaction between LARG-RH or LARG-RDP and Gα13 at equilibrium state and in transition states using Biacore T100

Interaction phase	Thermodynamic parameter	RH	RDP
Equilibrium	$\Delta G°$ [kJ mol^{-1}]	−43 ± 0.019	−47 ± 0.2
	$\Delta H°$ [kJ mol^{-1}]	−85 ± 0.8	−23 ± 8.6
	$\Delta S°$ [kJ mol^{-1} K^{-1}]	−0.14 ± 0.0027	0.079 ± 0.029
	$T\Delta S°$ [kJ mol^{-1}]	−43 ± 0.82	24 ± 8.8
	$\Delta Cp°$ [kJ mol^{-1} K^{-1}]	−5 ± 0.056	−3.8 ± 0.61
Association	$\Delta G°^{‡}$ [kJ mol^{-1}]	38 ± 0.19	36 ± 0.11
	$\Delta H°^{‡}$ [kJ mol^{-1}]	35 ± 4	61 ± 2.2
	$\Delta S°^{‡}$ [kJ mol^{-1} K^{-1}]	−0.01 ± 0.014	0.084 ± 0.0077
	$T\Delta S°^{‡}$ [kJ mol^{-1}]	−3 ± 4.2	25 ± 2.3
Dissociation	$\Delta G°^{‡}$ [kJ mol^{-1}]	82 ± 0.33	83 ± 0.24
	$\Delta H°^{‡}$ [kJ mol^{-1}]	50 ± 6.8	32 ± 4.6
	$\Delta S°^{‡}$ [kJ mol^{-1} K^{-1}]	−0.11 ± 0.024	−0.17 ± 0.016
	$T\Delta S°^{‡}$ [kJ mol^{-1}]	−32 ± 7.2	−52 ± 4.8

Thermodynamic parameters of the interactions were derived from the van't Hoff plots and Eyring plots in Fig. 4 and supplemental Fig. S5.

The LARG-RDP/$G\alpha_{13}$ interaction showed more negative free energy change ($\Delta G°$) than the LARG-RH/$G\alpha_{13}$ interaction,

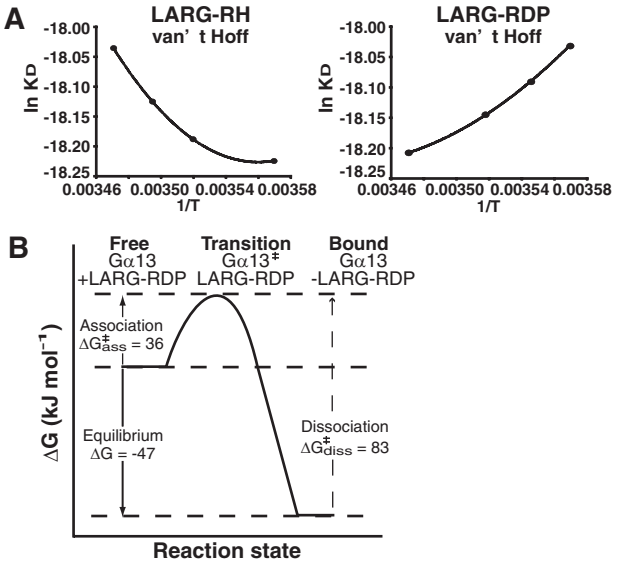

FIGURE 4. **Thermodynamic analysis of Gα13-LARG interaction.** *A*, thermodynamic analysis of the Gα13-LARG complex formation and dissociation through its RH and DH domain. van't Hoff plots and Eyring plots of the experimental data are shown. The thermodynamic parameters at an equilibrium state and at a transition state were estimated from van't Hoff plots and Eyring plots as described under "Experimental Procedures" (Table 2 and supplemental Fig. S3). *B*, schematic reaction profile of the thermodynamic energies at the different states of Gα13-LARG interaction.

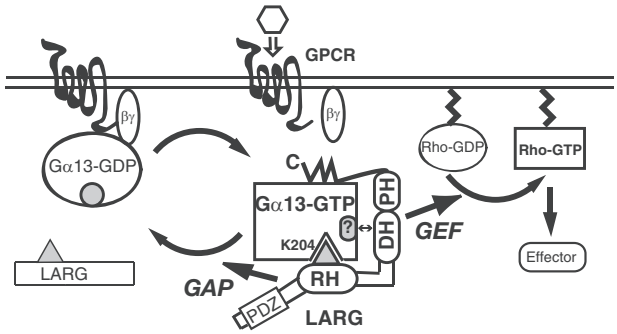

FIGURE 5. **A proposed model of Rho activation through Gα13-LARG interaction.** The interaction of LARG-RH with Gα13 activated by agonist-bound GPCR will induce conformational changes of DH/PH domains and C-terminal region to form an active Gα13-LARG complex.

which is consistent with the higher affinity of LARG-RDP *versus* LARG-RH (Table 2). In addition, thermodynamic parameters demonstrated the essential differences between the Gα13-RH interaction and Gα13-RDP interaction (Table 2). The binding of LARG-RH to Gα13 is enthalpy-driven and entropically unfavorable. In contrast, the binding of LARG-RDP to Gα13 is less favorable than that of LARG-RH from the enthalpy term but is entropy-driven with a positive ΔS°. In general, a large negative heat capacity change (Δ*C*p°) in a protein-protein interaction indicates the removal of water-accessible hydrophobic surface area coupled to conformational changes (25, 26). Δ*C*p° of 1 kJ mol^{-1} K^{-1} corresponds to the removal of ~990 $Å^2$ of exposed hydrophobic surface area (25, 26). Thus, a large negative Δ*C*p° of −3.8 kJ mol^{-1} K^{-1} together with the positive Δ*S*° (0.084 kJ mol^{-1} K^{-1}) suggests that >3500 $Å^2$ of hydrophobic surface is buried in the interface between Gα13 and the region between the RH domain and the DH/PH domains upon complex formation. Such extensive hydrophobic interactions would certainly stabilize the Gα13-LARG complex.

Furthermore, the free energy changes at the association and dissociation phases calculated by the Eyring theory were suitable for the equation $\Delta G^\circ = \Delta G^{\circ\ddagger}_{ass} - \Delta G^{\circ\ddagger}_{diss}$. A free energy barrier at the transition state of association between Gα13 and LARG-RDP was calculated as $\Delta G^{\circ\ddagger}_{ass}$ of 36 kJ mol^{-1}. The interaction between Gα13 and LARG-RDP will be driven by this binding free energy (Fig. 4*B*).

DISCUSSION

Dynamics of the Interaction between Gα13 and LARG with Large Conformational Rearrangements at the Interface—In this study, we have characterized the molecular mechanism of Gα13-LARG interaction by cellular and biochemical assays, including quantitative SPR analysis using a biosensor chip on which Gα13 was immobilized. Our results from the kinetic and thermodynamic analysis demonstrate that the simultaneous interaction of Gα13 through the RH domain, DH/PH domains, and C-terminal region of LARG facilitates the formation of the high affinity active Gα13/LARG complex. Furthermore, a large hydrophobic surface spanning >3500 $Å^2$ is created at the interface between Gα13 and the region between the RH domain and the DH/PH domains. It has been demonstrated by Spolar and Record (26) that the formation of a such large hydrophobic surface at the interface cannot be accounted for by association between pre-existing surfaces, but rather is coupled to conformational rearrangements between the proteins, most likely by induced fit. Thus, it appears unlikely that the binding of Gα13 to the RH domain uncovers a large pre-existing surface on the DH/PH domains that contacts Gα13 via hydrophobic interactions. The K204A mutation at the RH domain contact position in Gα13 resulted in large decreases in affinity for LARG fragments containing the RH domain (Fig. 1*C* and Table 1). This fact strongly supports the notion that lysine 204 is in the interface between Gα13 and LARG-RH and could be a hotspot for triggering significant conformational rearrangements in the binding site, which means that the interaction is most likely driven by an induced-fit mechanism. These results indicate that the interaction between Gα13 and LARG is induced through the binding of Gα13 with the RH domain and proceeds by burying an exposed hydrophobic surface to create a large complementary interface. Thus, both GAP and effector interfaces facilitate complex formation and activation of LARG (Figs. 4 and 5). A structural study has indicated that the N-terminal small region of the DH domain of LARG is necessary to exert GEF activity for Rho (27). Interestingly, this region has been shown to act as an activation "switch" for another RhoGEF, Vav. Therefore, it is possible that the association of the RH domain with Gα13 driven by an induced-fit mechanism directly or indirectly affects this region, and enables LARG to adopt the active conformation. Further x-ray crystal structure analysis of LARG or its complex with Gα13 will be necessary to clarify these points.

We have recently reported that p115RhoGEF interacts with Gα13 through separate surfaces for the GAP reaction and GEF activity regulation (16). In agreement with this finding, the K204A mutation does not affect the affinity of LARG-DH/PH or -DPC for $G\alpha_{i/13}$ (Fig. 1*C*), or stimulation of LARG's RhoGEF

activity in reconstitution assays (Fig. 2*F*) strongly suggesting the existence of an additional interface between $G\alpha_{13}$ and the DH/PH domains. Compared with a lock and key interaction, which proceeds via pre-existing complementary surfaces such as seen in the antigen-antibody interaction, the induced-fit mechanism will provide $G\alpha$ subunits with much more flexibility to interact with various downstream effectors. Similar to this finding, it was demonstrated recently that the $G\beta\gamma$ subunit interacts with a variety of downstream effectors using homologous interfaces containing hot spots (29–32). It is thus possible that other $G\alpha$-effector interactions may be regulated by a similar mechanism.

Our result using ALF_4^--activated $G\alpha_{13}$ represents the transition state of GTP hydrolysis. We have found that LARG-DH/PH has a higher affinity for $G\alpha_{13}$QL, which mimics the GTP-bound state, than for ALF_4^--activated $G\alpha_{13}$ (data not shown). In contrast, LARG-RH demonstrated the opposite affinity as previously demonstrated. The discrepancy between activation of LARG-DH/PH by $G\alpha_{13}$ in cell-based assays and reconstitution assays may result from the affinity difference of LARG-DH/PH for $G\alpha_{13}$QL and ALF_4^--activated $G\alpha_{13}$.

$G\alpha$/GAP/Effector Signaling Complex—We have demonstrated that the interaction of $G\alpha_{13}$ with LARG through the RH domain (a GAP interface) and the DH/PH domains (an effector interface) could coordinate together to stimulate the RhoGEF activity of LARG (Fig. 3, *A* and *B*). The spatial and kinetic connection of GAP and GEF activities within a LARG molecule may help to regulate amplification of G protein signaling, increase the temporal resolution of the response, and increase the specificity of the signal output. Because $G\alpha_{12/13}$ have characteristically slow rates of nucleotide exchange and GTP hydrolysis, this mechanism could be a rational system for $G\alpha_{12/13}$ signaling to regulate multiple important cellular functions with fast responses as well as long term processes (33, 34). Cooperative regulation of GAP and catalytic activities in one single effector molecule may also apply to other $G\alpha$ effectors such as PLCβ (35).

The simultaneous interaction of GAP and effector with activated $G\alpha$ has been clearly demonstrated with the crystal structure of the $G\alpha_t$-RGS9-PDEγ complex (36). The structure explains the mechanism by which PDEγ potentiates the GAP activity of RGS9-1: by increasing the affinity of RGS9-1 for $G\alpha_t$ to enhance the fidelity and temporal resolution of visual signal transduction (37, 38). Furthermore, the crystal structures of $G\alpha_q$-p63RhoGEF-RhoA and $G\alpha_q$-GRK2-$G\beta\gamma$, where the switch I region appears available for the simultaneous binding of RGS proteins, suggest that $G\alpha$ can bind an effector and a GAP at the same time (8, 39). Thus, simultaneous and non-overlapping binding of a GAP and an effector with $G\alpha$ may be a conserved mechanism to help efficiently regulate G protein-mediated signaling output.

It is also interesting to note that the $G\alpha_{13}$-RH interaction through the GAP interface may confer specificity on the $G\alpha_{13}$-LARG interaction through its effector interface (Fig. 3*A*). The result is analogous to the selective potentiation of the GAP activity of RGS9 for $G\alpha_t$ by PDEγ (40–42). The interaction of the RH domain with $G\alpha_{13}$ outside of the switch regions might contribute to determining the specificity of GEF activation by $G\alpha_{13}$ (7, 9). These results suggest that RGS proteins may play another important role in GPCR signaling pathways by specifying the effector molecule for $G\alpha$. We also demonstrated that activation of $G\alpha_{13}$ contributes to the subcellular redistribution of LARG from the cytosol to the plasma membrane through the interaction with its RH domain (Fig. 2*D*), which is consistent with the case of p115RhoGEF (5). This translocation will help LARG closely interact with its target, RhoA at the membrane.

Role of the C-terminal Region of LARG—Our kinetic studies indicate that the C-terminal region of LARG significantly affects the interaction with $G\alpha_{i/13}$, especially the dissociation of LARG from $G\alpha_{13}$ (Fig. 1*C* and Table 1), and regulates the $G\alpha_{13}$-stimulated RhoGEF activity of LARG (Fig. 3*D*). Our preliminary thermodynamic analysis of the LARG-RDPC/$G\alpha_{13}$ interaction could not produce an appropriate fitting to the theoretical curve, which suggests that the C-terminal region might be unstable, and some additional interacting protein may be required to stabilize the conformation upon binding to $G\alpha_{13}$ (supplemental Fig. 3*B*). Recently, the presence of homo- or hetero-oligomerization of RH-RhoGEFs through their C-terminal regions has been reported (43–45). However, the physiological function of this oligomerization process in cells has not yet been clearly understood. Further study is required to understand the functional role of the C-terminal region in the regulation of $G\alpha_{13}$-LARG signaling.

CONCLUSION

In this study we have characterized the molecular dynamics of $G\alpha_{13}$-effector interaction by applying both kinetic and thermodynamic analyses. The $G\alpha_{12/13}$-RhoGEF-Rho signaling pathway has been shown to participate in a variety of disease conditions, such as leukemia, cancer invasion, and hypertension (28, 46, 47). Detailed characterization of the mechanism of regulation of RH-RhoGEFs by $G\alpha_{13}$ as demonstrated in this study will contribute to the screening of novel drugs to control these diseases. X-ray crystallography structures of $G\alpha_{12/13}$ and the complex with target molecules has made progress toward understanding $G\alpha_{12/13}$-mediated signaling pathways (7, 9). However, it is essential to understand the molecular dynamics of the system to provide an active view of the protein-protein interactions during the signaling process. The combined efforts of the dynamic-interaction analysis such as SPR presented in this study together with the high resolution x-ray crystallography approach will be critical to further understand the molecular mechanism of this $G\alpha_{12/13}$-mediated signaling pathway.

Acknowledgment—We thank Yoshikazu Tanaka for help with thermodynamic analysis.

REFERENCES

1. Hepler, J. R., and Gilman, A. G. (1992) *Trends Biochem. Sci.* **17,** 383–387
2. Ross, E. M., and Wilkie, T. M. (2000) *Annu. Rev. Biochem.* **69,** 795–827
3. Zerangue, N., and Jan, L. Y. (1998) *Curr. Biol.* **8,** R313–316
4. Ross, E. M. (1989) *Neuron* **3,** 141–152
5. Bhattacharyya, R., and Wedegaertner, P. B. (2003) *Biochem. J.* **371,** 709–720
6. Wells, C. D., Gutowski, S., Bollag, G., and Sternweis, P. C. (2001) *J. Biol. Chem.* **276,** 28897–28905

7. Chen, Z., Singer, W. D., Sternweis, P. C., and Sprang, S. R. (2005) *Nat. Struct. Mol. Biol.* **12,** 191–197
8. Tesmer, V. M., Kawano, T., Shankaranarayanan, A., Kozasa, T., and Tesmer, J. J. (2005) *Science* **310,** 1686–1690
9. Kreutz, B., Yau, D. M., Nance, M. R., Tanabe, S., Tesmer, J. J., and Kozasa, T. (2006) *Biochemistry* **45,** 167–174
10. Fukuhara, S., Murga, C., Zohar, M., Igishi, T., and Gutkind, J. S. (1999) *J. Biol. Chem.* **274,** 5868–5879
11. Hart, M. J., Jiang, X., Kozasa, T., Roscoe, W., Singer, W. D., Gilman, A. G., Sternweis, P. C., and Bollag, G. (1998) *Science* **280,** 2112–2114
12. Kozasa, T., Jiang, X., Hart, M. J., Sternweis, P. M., Singer, W. D., Gilman, A. G., Bollag, G., and Sternweis, P. C. (1998) *Science* **280,** 2109–2111
13. Suzuki, N., Nakamura, S., Mano, H., and Kozasa, T. (2003) *Proc. Natl. Acad. Sci. U. S. A.* **100,** 733–738
14. Wells, C. D., Liu, M. Y., Jackson, M., Gutowski, S., Sternweis, P. M., Rothstein, J. D., Kozasa, T., and Sternweis, P. C. (2002) *J. Biol. Chem.* **277,** 1174–1181
15. Nakamura, S., Kreutz, B., Tanabe, S., Suzuki, N., and Kozasa, T. (2004) *Mol. Pharmacol.* **66,** 1029–1034
16. Kreutz, B., Hajicek, N., Yau, D. M., Nakamura, S., and Kozasa, T. (2007) *Cell Signal.* **19,** 1681–1689
17. Tanabe, S., Kreutz, B., Suzuki, N., and Kozasa, T. (2004) *Methods Enzymol.* **390,** 285–294
18. Horn, J. R., Russell, D., Lewis, E. A., and Murphy, K. P. (2001) *Biochemistry* **40,** 1774–1778
19. Krogsgaard, M., Prado, N., Adams, E. J., He, X. L., Chow, D. C., Wilson, D. B., Garcia, K. C., and Davis, M. M. (2003) *Mol. Cell* **12,** 1367–1378
20. Wear, M. A., and Walkinshaw, M. D. (2006) *Anal. Biochem.* **359,** 285–287
21. Roos, H., Karlsson, R., Nilshans, H., and Persson, A. (1998) *J. Mol. Recognit.* **11,** 204–210
22. Coleman, D. E., Berghuis, A. M., Lee, E., Linder, M. E., Gilman, A. G., and Sprang, S. R. (1994) *Science* **265,** 1405–1412
23. Ren, X. D., and Schwartz, M. A. (2000) *Methods Enzymol.* **325,** 264–272
24. Aragay, A. M., Collins, L. R., Post, G. R., Watson, A. J., Feramisco, J. R., Brown, J. H., and Simon, M. I. (1995) *J. Biol. Chem.* **270,** 20073–20077
25. Murphy, K. P., Bhakuni, V., Xie, D., and Freire, E. (1992) *J. Mol. Biol.* **227,** 293–306
26. Spolar, R. S., and Record, M. T., Jr. (1994) *Science* **263,** 777–784
27. Kristelly, R., Gao, G., and Tesmer, J. J. (2004) *J. Biol. Chem.* **279,** 47352–47362
28. Wirth, A., Benyo, Z., Lukasova, M., Leutgeb, B., Wettschureck, N., Gorbey, S., Orsy, P., Horvath, B., Maser-Gluth, C., Greiner, E., Lemmer, B., Schutz, G., Gutkind, J. S., and Offermanns, S. (2008) *Nat. Med.* **14,** 64–68
29. Bonacci, T. M., Mathews, J. L., Yuan, C., Lehmann, D. M., Malik, S., Wu, D., Font, J. L., Bidlack, J. M., and Smrcka, A. V. (2006) *Science* **312,** 443–446
30. Ghosh, M., Peterson, Y. K., Lanier, S. M., and Smrcka, A. V. (2003) *J. Biol. Chem.* **278,** 34747–34750
31. Johnston, C. A., Willard, F. S., Jezyk, M. R., Fredericks, Z., Bodor, E. T., Jones, M. B., Blaesius, R., Watts, V. J., Harden, T. K., Sondek, J., Ramer, J. K., and Siderovski, D. P. (2005) *Structure* **13,** 1069–1080
32. Scott, J. K., Huang, S. F., Gangadhar, B. P., Samoriski, G. M., Clapp, P., Gross, R. A., Taussig, R., and Smrcka, A. V. t. (2001) *EMBO J.* **20,** 767–776
33. Kozasa, T., and Gilman, A. G. (1995) *J. Biol. Chem.* **270,** 1734–1741
34. Singer, W. D., Miller, R. T., and Sternweis, P. C. (1994) *J. Biol. Chem.* **269,** 19796–19802
35. Berstein, G., Blank, J. L., Jhon, D. Y., Exton, J. H., Rhee, S. G., and Ross, E. M. (1992) *Cell* **70,** 411–418
36. Slep, K. C., Kercher, M. A., He, W., Cowan, C. W., Wensel, T. G., and Sigler, P. B. (2001) *Nature* **409,** 1071–1077
37. He, W., Cowan, C. W., and Wensel, T. G. (1998) *Neuron* **20,** 95–102
38. Skiba, N. P., Hopp, J. A., and Arshavsky, V. Y. (2000) *J. Biol. Chem.* **275,** 32716–32720
39. Lutz, S., Shankaranarayanan, A., Coco, C., Ridilla, M., Nance, M. R., Vettel, C., Baltus, D., Evelyn, C. R., Neubig, R. R., Wieland, T., and Tesmer, J. J. (2007) *Science* **318,** 1923–1927
40. McEntaffer, R. L., Natochin, M., and Artemyev, N. O. (1999) *Biochemistry* **38,** 4931–4937
41. Skiba, N. P., Yang, C. S., Huang, T., Bae, H., and Hamm, H. E. (1999) *J. Biol. Chem.* **274,** 8770–8778
42. Sowa, M. E., He, W., Wensel, T. G., and Lichtarge, O. (2000) *Proc. Natl. Acad. Sci. U. S. A.* **97,** 1483–1488
43. Eisenhaure, T. M., Francis, S. A., Willison, L. D., Coughlin, S. R., and Lerner, D. J. (2003) *J. Biol. Chem.* **278,** 30975–30984
44. Chikumi, H., Barac, A., Behbahani, B., Gao, Y., Teramoto, H., Zheng, Y., and Gutkind, J. S. (2004) *Oncogene* **23,** 233–240
45. Grabocka, E., and Wedegaertner, P. B. (2007) *Mol. Pharmacol.* **72,** 993–1002
46. Kelly, P., Moeller, B. J., Juneja, J., Booden, M. A., Der, C. J., Daaka, Y., Dewhirst, M. W., Fields, T. A., and Casey, P. J. (2006) *Proc. Natl. Acad. Sci. U. S. A.* **103,** 8173–8178
47. Kourlas, P. J., Strout, M. P., Becknell, B., Veronese, M. L., Croce, C. M., Theil, K. S., Krahe, R., Ruutu, T., Knuutila, S., Bloomfield, C. D., and Caligiuri, M. A. (2000) *Proc. Natl. Acad. Sci. U. S. A.* **97,** 2145–2150